The efficiency of transport into the stratosphere via the Asian and North American summer monsoon circulations

Xiaolu Yan[1], Paul Konopka[1], Felix Ploeger[1], Aurélien Podglajen[1], Jonathon S. Wright[2], Rolf Müller[1], and Martin Riese[1]

[1]Forschungszentrum Jülich (IEK-7: Stratosphere), Jülich, Germany
[2]Department of Earth System Science, Tsinghua University, Beijing, China

Correspondence: Xiaolu Yan (x.yan@fz-juelich.de)

Abstract. Transport of pollutants into the stratosphere via the Asian summer monsoon (ASM) or North American summer monsoon (NASM) may affect the atmospheric composition and climate both locally and globally. We identify and study the robust characteristics of transport from the ASM and NASM regions to the stratosphere using the Lagrangian chemistry transport model CLaMS as driven by the ERA-Interim and MERRA-2 reanalyses. In particular, we investigate the relative

5 influences of the ASM and NASM on stratospheric composition, the transport pathways by which these influences are effected, and the quantitative contributions and efficiencies of transport from different altitudes in these two monsoon regions to the stratosphere. We release artificial tracers in several vertical layers from the middle troposphere to the lower stratosphere in both ASM and NASM source regions during July and August 2010−2013 and track their evolution until the following summer. We find that the magnitude of transport from the ASM and NASM regions to the tropical stratosphere, and even to the Southern

10 Hemispheric stratosphere, is higher when the tracers are released at the 350−360 K level. For tracers released close to the tropopause (370−380 K), transport is primarily into the Northern Hemispheric stratosphere. Results for different vertical layers or air origin reveal two transport pathways from the upper troposphere over the ASM and NASM regions to the tropical pipe: (i) quasi-horizontal transport to the tropics below the tropopause followed by ascent to the stratosphere via tropical upwelling, and (ii) ascent into the stratosphere inside the ASM/NASM followed by quasi-horizontal transport to the tropical lower stratosphere

15 and tropical pipe. The tropical pathway (i) is faster than the monsoon pathway (ii), particularly in the ascending branch. Ultimately, the abundance of air in the tropical pipe that originates in the ASM upper troposphere (350−360 K, ∼5%) is comparable to that of air ascending directly from the tropics ten months after the release of the source tracers. By contrast, the air mass contributions from the ASM to the tropical pipe are about three times larger than the corresponding contribution from the NASM (∼1.5%). The transport efficiency into the tropical pipe, normalized by the mass of the domain, is greatest

20 from the ASM region at 370−380 K. Transport from the ASM to the tropical pipe is almost twice as efficient as transport from the NASM or tropics to the tropical pipe. Although the contribution from the NASM to the stratosphere is less than that from either the ASM or the tropics, the transport efficiency from the NASM is comparable to that from the tropics.

1 Introduction

The structure and composition of the upper troposphere and lower stratosphere (UTLS) during boreal summer and fall over Asia
and North America have many unique features. The Asian summer monsoon (ASM) and North American summer monsoon
(NASM) anticyclones are not only important locally, but also affect first the entire northern hemisphere (NH) and then the
whole atmosphere (Vogel et al., 2016; Ploeger et al., 2017; Yu et al., 2017; Vogel et al., 2019). These circulations pump vast
amounts of water vapor and other chemical constituents from the surface to the UTLS (Gettelman et al., 2004a; Randel et al.,
2010). Air originating in the ASM and NASM is lifted high enough to ascend freely into the stratosphere and can be transported
to distant locations (Liang et al., 2004), where it may exert considerable influences on stratospheric chemistry, radiation and
dynamics (Vogel et al., 2016). Hence, transport of air uplifted by the ASM and NASM is an important factor influencing the
composition of the UTLS and the evolution of global climate.

Transport via the ASM has drawn extensive attention. This transport involves deep convection uplifting air from the bound-
ary layer to the UTLS (Fu et al., 2006; Randel et al., 2010; Wright et al., 2011; Bergman et al., 2012; Fadnavis et al., 2015;
Santee et al., 2017), including the injection of boundary layer air by typhoons over Southeast Asia and Western Pacific into the
outer regions of the ASM anticyclone (Vogel et al., 2014; Li et al., 2018). At higher levels, transport is dominated by the strong
ASM anticyclone (Randel and Park, 2006; Park et al., 2009), which is confined by easterly (on the tropical side) and westerly
(on the extratropical side) jets. These jets act as strong transport barriers and restrict isentropic mixing (Ploeger et al., 2015;
Poshyvailo et al., 2018). High concentrations of tropospheric tracers and low concentrations of stratospheric tracers within the
anticyclone are evident in a variety of observations (Park et al., 2008; Randel et al., 2010; Vogel et al., 2014; Ungermann et al.,
2016; Santee et al., 2017). A fraction of the air within the ASM anticyclone eventually enters the tropical pipe (TrP) and the NH
extratropical lowermost stratosphere like a vertical 'chimney' and an isentropic 'blower' (Pan et al., 2016; Ploeger et al., 2017).
The processes involved in this transport affect the chemical composition of the UTLS, including the buildup of ozone precur-
sors (Fadnavis et al., 2015) and the Asian tropopause aerosol layer (ATAL) (Vernier et al., 2011; Yu et al., 2017; Vernier et al.,
2018; Brunamonti et al., 2018). The latter has been estimated to cause a significant regional radiative cooling of the Earth's
surface with an intensity of $\sim 0.1\,\mathrm{W\,m^{-2}}$ (Vernier et al., 2011, 2015).

In comparison to the ASM, transport to the stratosphere via the NASM has received relatively little scientific attention to
date. Chen (1995) found that significant stratosphere-troposphere exchange (STE) occurs at potential temperature greater than
340 K in the NH during boreal summer and linked this exchange with the ASM and NASM circulations. Dunkerton (1995)
reported that the influence of monsoon circulations on STE vanishes above $\sim$25 km. Water vapor retrievals from the Halogen
Occultation Experiment (HALOE) satellite revealed two pronounced maxima over Asia and North America, presumably re-
lated to monsoon-driven convection over these two regions (Dethof et al., 1999; Randel et al., 2001). Dessler and Sherwood
(2004) pointed out that summer convection over North America is sufficient to exert a significant effect on the water vapor bud-
get, although not on the ozone budget. Gettelman et al. (2004b) argued that the NASM may entrain air from the high latitude
troposphere into the subtropical lower stratosphere but this air would rarely reach the deep tropics. However, using satellite
observations, Randel et al. (2012) linked a positive anomaly in the deuterium content of lower stratospheric water vapor to the
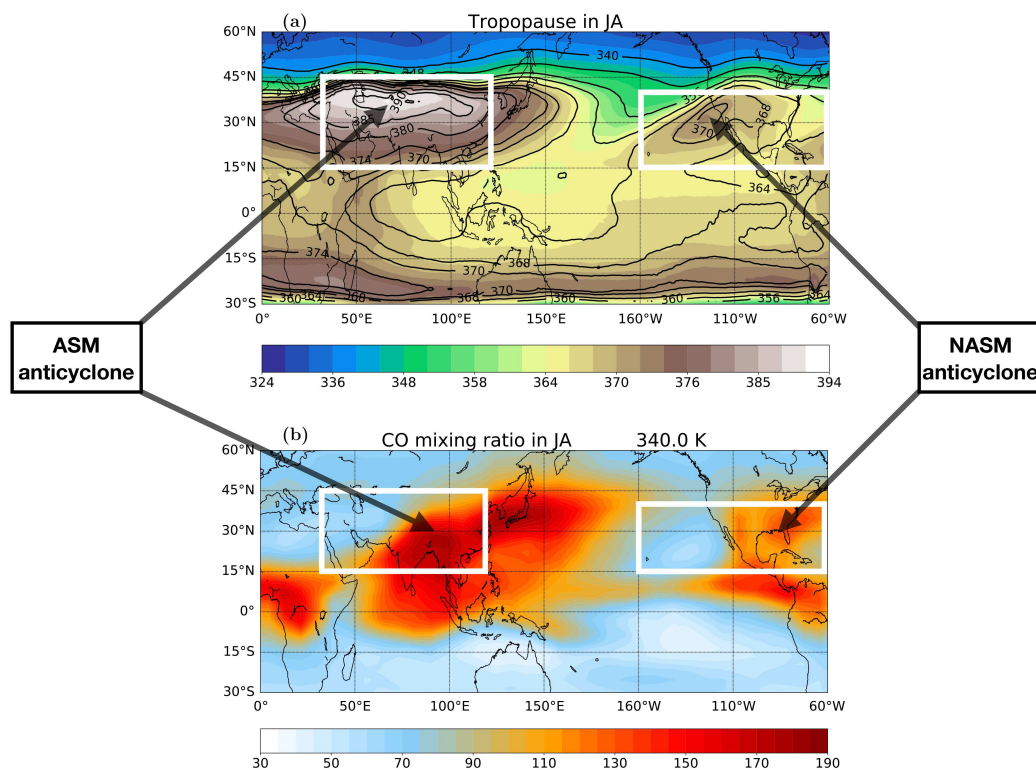
Figure 1. (a): Climatologies of the tropopause (lapse rate) potential temperature (in K) from ERA-Interim (1979−2016, color shading) and MERRA-2 (1980−2016, contours) for July and August. (b): Climatologies of CO (in ppbv) at θ=340 K calculated from MLS (2004−2016) for July and August. Map is created by python.

NASM (and not the ASM) and showed that this anomaly extends into the tropics. Meanwhile, model simulations driven by ERA-Interim reanalysis products suggest that the fraction of NASM air in NH midlatitudes is about one order of magnitude smaller than the fraction of ASM air (Ploeger et al., 2013).

60   Figure 1a shows clear anticyclonic circulations associated with higher tropopause levels over the ASM and NASM regions during July−August based on both the ERA-Interim and MERRA-2 reanalyses. Correspondingly, measurements of CO from the Aura Microwave Limb Sounder (MLS) show high values at 340 K over the ASM and NASM regions (Fig. 1b). As described above, most previous studies have focused on the transport pathways related to the ASM anticyclone, with relatively few contributions related to the transport via the NASM anticyclone. In this study, we address the following questions:

65 (1) How does transport from the ASM and NASM affect stratospheric composition?

(2) How large are contributions from the ASM and NASM regions to the stratosphere relative to contributions from the inner tropics?

(3) From which levels within the ASM and NASM regions do the most effective transport pathways to the stratosphere originate?

70   Studies of air mass transport across the tropopause often rely on winds and diabatic heating rates from reanalyses. Diabatic heating rates, especially if derived from reanalyses, are more suitable to quantify vertical transport than the pressure tendencies, which are strongly affected by the numerical noise of the assimilation procedure (Eluszkiewicz et al., 2000; Schoeberl et al., 2003). However, diabatic heating rates are highly uncertain, and differ substantially among reanalyses (Randel and Jensen, 2013; Wright and Fueglistaler, 2013; Abalos et al., 2015). These differences have important implications for transport calcu-

75   lations in the UTLS (Wright et al., 2011; Schoeberl et al., 2012; Bergman et al., 2013; Wang et al., 2014; Abalos et al., 2015; Ploeger et al., 2019; Tao et al., 2019). To evaluate the robust characteristics of transport in different reanalyses, we use both the ERA-Interim and MERRA-2 reanalyses to drive the Lagrangian transport model CLaMS. We then investigate the pathways for air mass transport from the ASM and NASM anticyclone into the lower stratosphere and quantify the associated transport efficiencies (TE) and the amounts of stratospheric air originating from each source region using both sets of simulations. In

80   Sect. 3, we discuss reanalysis-related differences in the statistics of transport from monsoon regions to the lower stratosphere and TrP and investigate the influences of the ASM and NASM on stratospheric composition (e.g. HCN and water vapor). In Sect. 4, we assess the efficiency of transport to the stratosphere via the ASM and NASM anticyclones. We discuss our findings in Sect. 5 before closing with a brief summary of the key results.

2   Data and methods

85   We apply tracer-independent diagnostics (i.e. without chemistry and emissions) to quantify air mass transport through the ASM anticyclone, NASM anticyclone and tropics. All diagnostics are based on simulations using the Lagrangian chemistry transport model CLaMS (McKenna et al., 2002; Konopka et al., 2004; Pommrich et al., 2014). The model transport is driven by horizontal winds and total diabatic heating rates from either the ERA-Interim (CLaMS-EI) or MERRA-2 (CLaMS-M2) reanalysis. The use of two reanalysis data sets provides important constraints on the range of possible outcomes and potential

90   biases associated with differences in horizontal winds and total diabatic heating rates between these two reanalyses.

We include air mass origin tracers in the model to diagnose the fraction of air at any location in the stratosphere which left either of the monsoon anticyclones or the tropics during the previous boreal summer monsoon season. There are several ways to define the ASM anticyclone including Montgomery stream function (Santee et al., 2017), stream function (Yan et al., 2018; Tweedy et al., 2018), geopotential height (Pan et al., 2016) and potential vorticity (PV; Ploeger et al., 2017). Applying similar

95   criteria to the NASM is less straightforward.

Here, we follow the geographic definition of the ASM source region proposed by Yu et al. (2017), which covers the domain [15° N, 45° N, 30° E, 120° E]. Within this region, we consider several different layers that cover the atmospheric column from the middle troposphere to the UTLS. For the layer spanning $370-380\,\mathrm{K}$ potential temperature, our results are very similar to those of Ploeger et al. (2017), who used a PV-based approach to define the anticyclone (detailed comparisons are provided

100   below). We therefore elect to use this simple geographical domain to represent the ASM region. One of the motivations for this

approach is that it offers direct analogues for the NASM region [15° N, 40° N, 160° W, 60° W] and the tropics [15° S, 15° N]. Note that the use of either a regular box or a PV contour to define the ASM region yields very similar results, as shown by Garny and Randel (2016). Vertically, we divide the column of air from the middle troposphere to the lower stratosphere above each region into 4 potential temperature layers $340-350\,\mathrm{K}$, $350-360\,\mathrm{K}$, $360-370\,\mathrm{K}$ and $370-380\,\mathrm{K}$ with i labeling the layer.

105
$$M_{\mathrm{ASM}}^{i}(\lambda,\phi,\theta,t) = \begin{cases} 1 & \lambda \in [30°\,\mathrm{E},\,120°\,\mathrm{E}],\ \phi \in [15°\,\mathrm{N},\,45°\,\mathrm{N}],\ \theta \in \mathrm{Box}_i,\ \text{and t} \in [\text{July, August}] \\ 0 & \text{elsewhere} \end{cases}$$

$$M_{\mathrm{NASM}}^{i}(\lambda,\phi,\theta,t) = \begin{cases} 1 & \lambda \in [160°\,\mathrm{W},\,60°\,\mathrm{W}],\ \phi \in [15°\,\mathrm{N},\,40°\,\mathrm{N}],\ \theta \in \mathrm{Box}_i,\ \text{and t} \in [\text{July, August}] \\ 0 & \text{elsewhere} \end{cases}$$

$$M_{\mathrm{Tropics}}^{i}(\lambda,\phi,\theta,t) = \begin{cases} 1 & \lambda \in [180°\,\mathrm{W},\,180°\,\mathrm{E}],\ \phi \in [15°\,\mathrm{S},\,15°\,\mathrm{N}],\ \theta \in \mathrm{Box}_i,\ \text{and t} \in [\text{July, August}] \\ 0 & \text{elsewhere} \end{cases}$$

Here $M_{\mathrm{ASM}}^{i}(\lambda,\phi,\theta,\mathrm{t})$, $M_{\mathrm{NASM}}^{i}(\lambda,\phi,\theta,\mathrm{t})$ and $M_{\mathrm{Tropics}}^{i}(\lambda,\phi,\theta,\mathrm{t})$ mark air mass fractions in the three-dimensional domains where the artificial air fraction is set to 1 on each day during July−August in CLaMS simulations covering the period from
110 2010 to 2013. The symbols λ, ϕ and t represent longitude, latitude and time, respectively. The tracer is set to zero everywhere on 1 July of each year and is set to 1 inside the source domains for this and every subsequent day through 31 August of that same year. The artificial tracer is advected as an inert tracer outside the source domains, as well as inside the source domains after the release. The tracer mixing ratio at any location in the stratosphere equals the fraction of air which left the corresponding source layer in the ASM, NASM or tropical domain during previous monsoon season (see also Orbe et al. 2013; Ploeger et al.
115 2017). After releasing the tracer in each box, we track the primary transport pathway and associated transport efficiencies from each source region to the global stratosphere, focusing especially on transport to the tropical pipe (TrP), the extratropical lower stratosphere in the Southern Hemisphere (LS-SH), and the extratropical lower stratosphere in the Northern Hemisphere (LS-NH). This experimental setup is illustrated in Fig. 2.

Observations of the tropospheric tracer HCN obtained from the Atmospheric Chemistry Experiment Fourier Transform
120 Spectrometer (ACE-FTS) satellite instrument (Bernath et al., 2005) are used to validate the monsoon air mass tracer. These data have been presented and discussed by Randel et al. (2010) and Ploeger et al. (2017). Here, we use HCN from ACE-FTS level 2 data version 3.6 (Boone et al., 2005, 2013) to investigate the correspondence between pollutants in the stratosphere and transport via both monsoons. In addition, MLS version 4 retrievals of CO (Livesey et al., 2018) are used to investigate the influence of the monsoon anticyclones on the tracer distribution as shown in Fig. 1b, and MLS version 4 retrievals of
125 water vapor are used to diagnose vertical and horizontal transport of tracer from the monsoon regions and its influence on stratospheric composition.
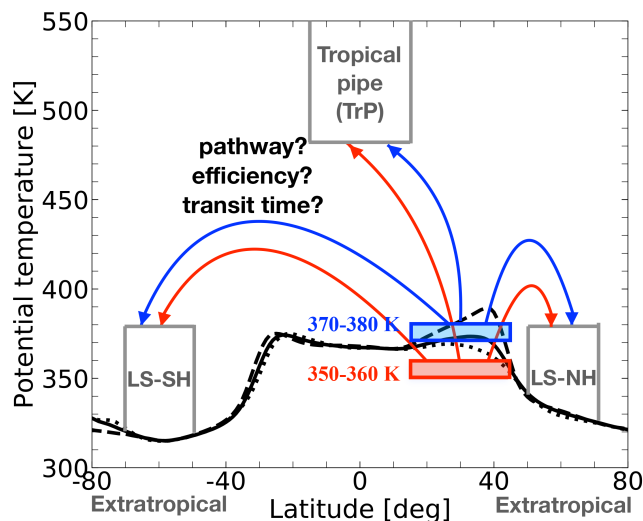
Figure 2. Definition of source regions (Box$_i$) at $350-360$ K (red) and $370-380$ K (blue). The following three destination regions (i.e. regions where transport statistics from the source regions are diagnosed) are considered: the tropical pipe (TrP: $15°$ S$-15°$ N), the extratropical lower stratosphere in the Southern Hemisphere (LS-SH: $50°$ S$-70°$ S), and the extratropical lower stratosphere in the Northern Hemisphere (LS-NH: $50°$ N$-70°$ N). The black solid, dashed and dotted lines respectively mark the zonal-mean, ASM and NASM tropopause (lapse rate) from ERA-Interim averaged over July$-$August $2010-2013$.

3 Transport pathways into the stratosphere and influence on stratospheric composition

3.1 Zonal-mean perspective on transport

Figure 3 shows the average air mass fraction from ASM and NASM regions initialized in the $350-360$ K (Fig. 3a and Fig. 3b) and $370-380$ K (Fig. 3c and Fig. 3d) layers in July and August of $2010-2013$ in the CLaMS-EI simulations during the following April$-$June, about ten months after the release of the tracers. Air is transported to the global stratosphere from both the ASM and the NASM. However, much more monsoon air originates from the ASM region than from the NASM region, and ASM air is transported to a higher level in the TrP by the following April$-$June when compared to NASM air. More monsoon tracer is transported into the stratosphere from the $350-360$ K layer than from the $370-380$ K layer for both the ASM and NASM regions. Monsoon air initialized at $350-360$ K is more prevalent in the SH stratosphere than in the NH, while monsoon air initialized at $370-380$ K is more likely to remain in the NH. The distribution of the monsoon tracer initialized at $340-350$ K (not shown) is also skewed toward the SH, similar to the results for $350-360$ K, while the distribution of the monsoon tracer from $360-370$ K is more symmetric between the hemispheres. In summary, during the following April$-$June, the monsoon tracers are more likely to end up in the SH stratosphere if they are initialized at lower levels ($340-350$ K or $350-360$ K), and more likely to end up in the NH stratosphere if they are initialized at higher levels ($360-370$ K or $370-380$ K). To avoid redundancy, we only show the results for tracers initialized in the $350-360$ K and $370-380$ K layers in this paper.
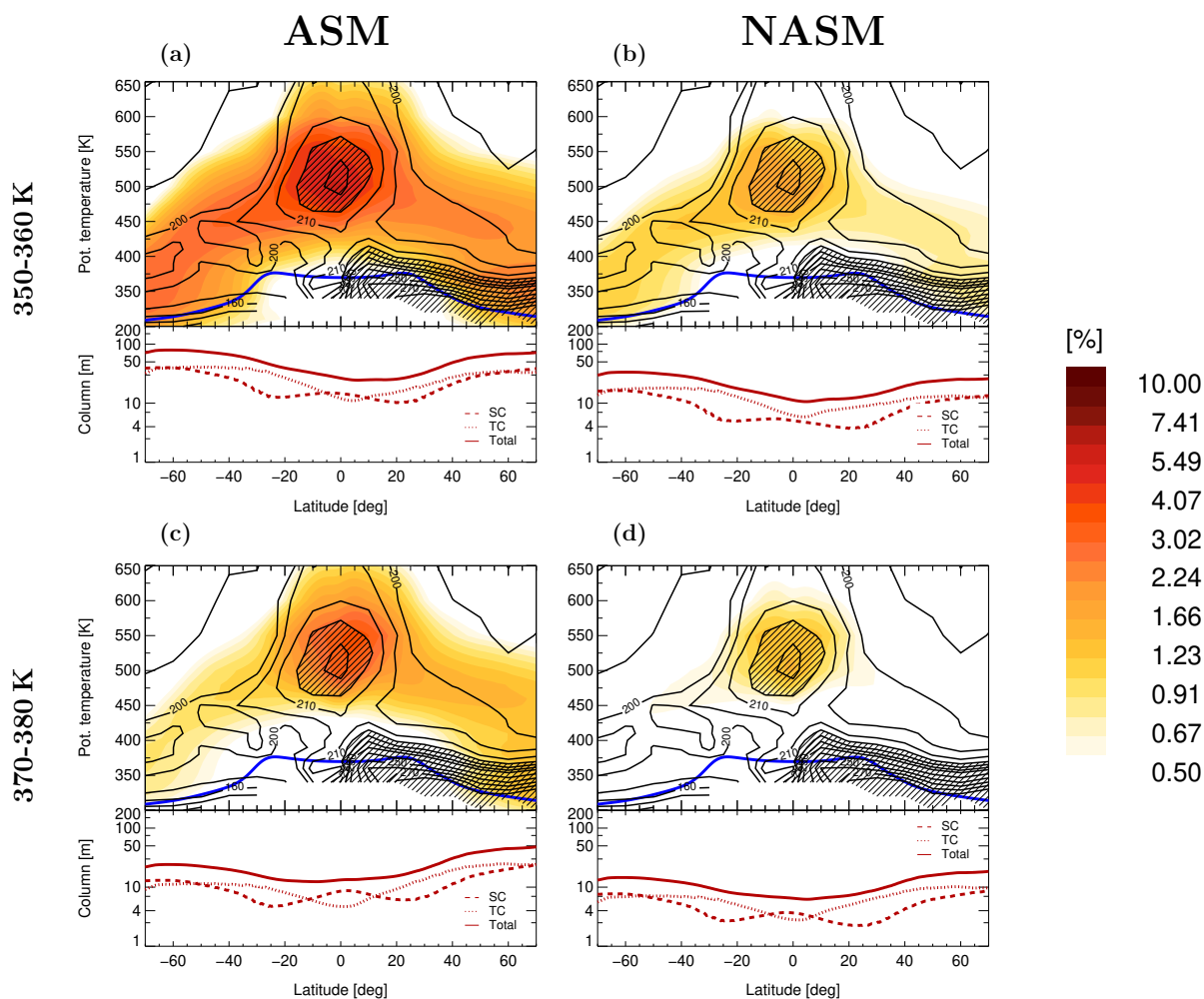
Figure 3. Climatological (2010−2013) zonal mean air mass fraction from the ASM (a and c) and the NASM (b and d) initialized at 350−360 K (upper) and 370−380 K (lower) in CLaMS-EI (color shading) during the following April−June. HCN from ACE-FTS observations (black contours) is also shown for context. Regions with HCN volume mixing ratios greater than 215 pptv are hatched. Blue lines mark the lapse rate tropopause. The red lines show column integrals (thickness: in m) of the monsoon tracer above the tropopause (SC: dashed), below the tropopause (TC: dotted) and through the entire atmosphere (solid). (Note the logarithmic color scale.)

Ploeger et al. (2017) showed that the simulated ASM tracer based on driving CLaMS with ERA-Interim correlates well with ACE-FTS observations of HCN. Here, we find that the HCN observations show strong correlations with both the ASM and NASM tracers in the TrP. This result suggests that both monsoon regions could serve as sources of enhanced HCN to the

145   stratosphere, with the ASM region representing a relatively strong source and the NASM region representing a relatively weak source. Although the HCN mixing ratio over the NASM is lower than that over the ASM, it is much higher than that over the tropics (Randel et al., 2010, their Fig. 1). The peak HCN mixing ratios in the TrP closely overlap with the peak contributions of monsoon tracers initialized in the $350-360$ K layer, and are located slightly below the peak contributions of monsoon tracers initialized at $370-380$ K. However, such vertical offsets should be interpreted with caution given likely overestimates

150   of tropical upwelling in ERA-Interim (Dee et al., 2011; Wright and Fueglistaler, 2013; Ploeger et al., 2019; Tao et al., 2019).

Column integrals are calculated to further investigate the transport of the monsoon tracers. These integrals are defined as the thickness (in units of m) of pure monsoon air assuming standard temperature and pressure for each altitude. Column integrals of monsoon air above the tropopause (SC), below the tropopause (TC), and through the entire atmosphere are shown along the bottom of each panel in Fig. 3. The column integrals of ASM and NASM tracers show similar patterns in both hemispheres.

155   The TC, SC, and total monsoon tracer columns initialized at $350-360$ K show larger values in the SH. The larger columns in the SH originating from the $350-360$ K layer over the monsoon regions may arise from a combination of three effects: weaker confinement of air inside the monsoon regions at this layer, hemispheric differences in isentropic mixing, and the seasonality of the Brewer-Dobson circulation. A portion of the monsoon tracers initialized at the $350-360$ K level enter the tropics due to wave-driven isentropic transport and are then advected into the SH through the shallow branch of the Brewer-

160   Dobson circulation (Rosenlof, 1995; Konopka et al., 2015). By contrast, monsoon tracers released in the $370-380$ K layer are more tightly confined to the NH, with higher column-integrated values for both the troposphere and stratosphere in the NH.

Figure 4 shows the air fraction during the following April$-$June for the ASM and NASM tracers initialized at $350-360$ K and $370-380$ K in July$-$August based on CLaMS-M2 simulations. Similar to the results from CLaMS-EI, the fraction of ASM air is larger than that of NASM air in the TrP, and the ASM air reaches a higher vertical level. More monsoon tracer is

165   transported into the stratosphere from lower levels than from higher levels, and the distributions of monsoon tracers also show hemispheric asymmetries similar to those in the CLaMS-EI case. However, despite these many similarities, the CLaMS-M2 simulations show much larger proportions of ASM and NASM air in the global stratosphere in comparison to those from CLaMS-EI. Another prominent difference concerns the vertical transport of monsoon air. The tracer peak from CLaMS-M2 is slightly below the HCN peak from satellite observations for tracers initialized at both the lower and the upper layers. This

170   can be attributed to slower upwelling, which stems from smaller diabatic heating rates in the lower stratosphere in MERRA-2 (Ploeger et al., 2019; Tao et al., 2019). Slower upwelling leads to larger contributions from quasi-horizontal transport and smaller contributions from vertical transport relative to the CLaMS-EI simulations. Transport of tracers into the stratosphere takes a longer time in the CLaMS-M2 simulations but a larger fraction of monsoon air reaches and remains in the stratosphere. Column-integrated monsoon tracer values from CLaMS-M2 are also much larger than those from CLaMS-EI. This difference

175   arises in part because monsoon tracers from CLaMS-M2 reach relatively lower levels in the stratosphere by the following
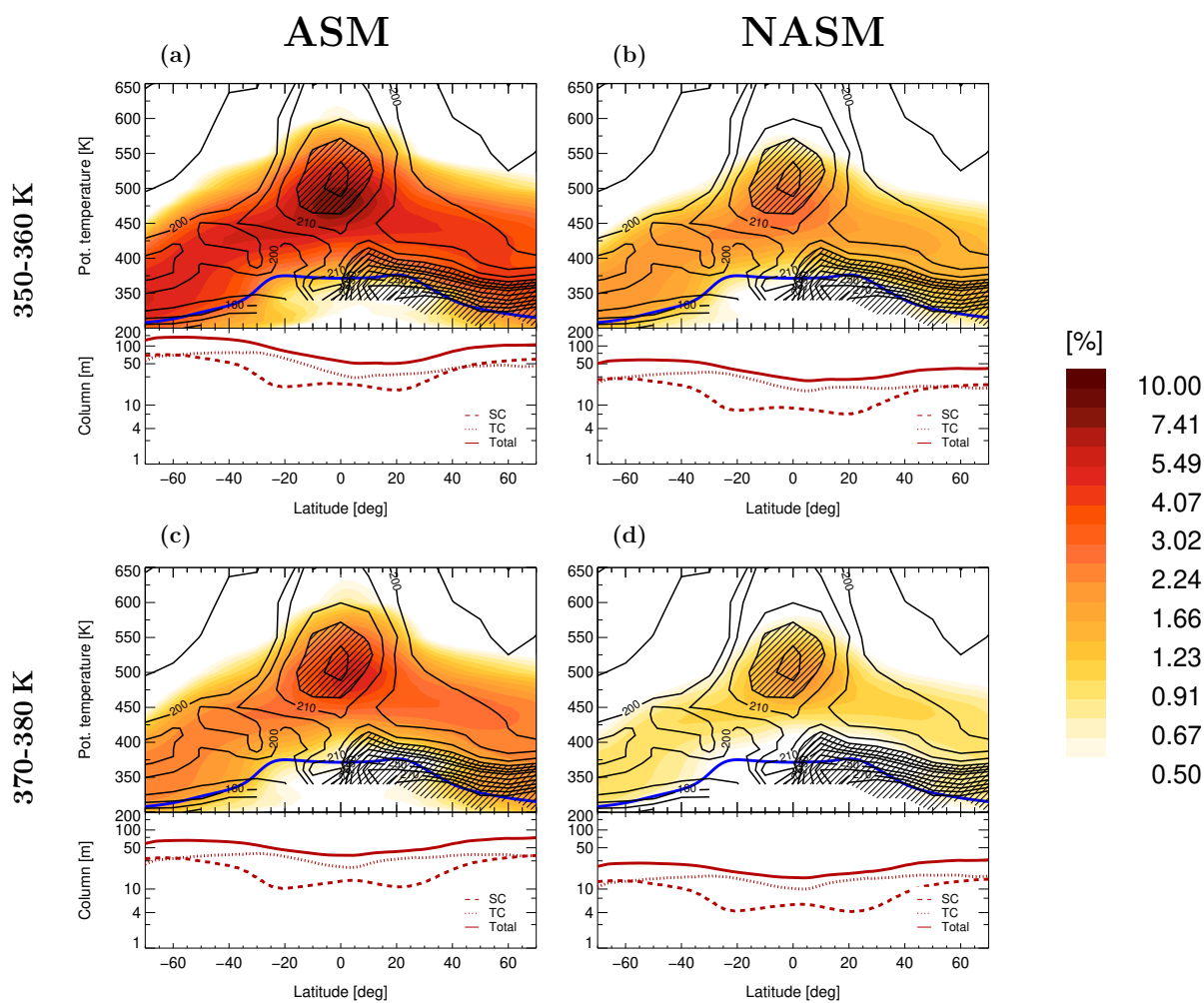
Figure 4. Same as Fig. 3 but for CLaMS-M2.

April−June compared to those from CLaMS-EI and air density is larger at lower levels. Differences between the SH and NH for monsoon tracers initialized in 370−380 K layer are smaller than those based on CLaMS-EI (not shown).

3.2 Two distinct transport pathways

In Sec. 3.1, we reported distinct differences in transport into the stratosphere between the ASM and the NASM and between two different vertical levels of the monsoon source regions in the upper troposphere (the 350−360 K and 370−380 K layers). The differences in simulated transport of monsoon tracers released at different vertical levels imply the existence of multiple transport pathways from the monsoon source regions to the TrP. Along the first pathway, termed 'tropical pathway' in the following, the tracer is first horizontally advected to the tropics, where it ascends through the tropical tropopause layer (TTL) into the TrP. Along the second pathway, termed 'monsoon pathway' in the following, the tracer is first lifted across the tropopause within the monsoon anticyclone and then transported isentropically to the tropical lower stratosphere and TrP. In this section, we endeavour to disentangle these two pathways and clarify the extent of transport from the monsoon source regions to the global stratosphere by separating the contributions of vertical transport within the tropics from those of horizontal transport into the tropics. We also compare the artificial tracers from the model simulations with MLS water vapor observations and CLaMS-simulated water vapor to investigate the influence of the monsoons on stratospheric chemical composition.

The vertical transport of ASM and NASM air into the tropical stratosphere ($15°$ S−$15°$ N) in CLaMS-EI is illustrated using the familiar 'tape-recorder' form (Mote et al., 1996) in Fig. 5. The transport barrier between the tropics and subtropics is weaker during boreal summer (Chen, 1995; Haynes and Shuckburgh, 2000). Monsoon tracers released at lower levels are especially abundant in the tropical UTLS during summer, indicating that a large fraction of the monsoon air from 350−360 K that reaches the TrP may be advected quasi-horizontally into the tropics before ascending. We also find that less of the monsoon tracer reaches the tropics when it is initialized at higher levels relative to when it is initialized at lower levels. This difference suggests that tracers initialized at higher levels within the monsoon regions primarily ascend locally before being mixed or advected into the tropics. ASM air rises slightly faster than NASM air and reaches slightly higher altitudes by the end of the simulation period. These features are consistent with the results discussed above.

MLS water vapor observations are included for additional context in Fig. 5. The annual mean of MLS water vapor is removed to highlight the annually-repeating water vapor tape recorder. The simulated ASM and NASM tracers correlate well with the 'wet' phase of the tape recorder (positive anomalies after removing the annual mean), which starts each year in boreal summer. The close correspondence between the monsoon air mass tracers and the 'wet' phase of the water vapor tape recorder in the tropics is consistent with the idea that the ASM and NASM contribute to moistening the tropical lower stratosphere during boreal summer (Fu et al., 2006; Randel et al., 2012). Note however that large concentrations of monsoon tracers in the tropics do not always correlate with large water vapor mixing ratios in the tropical UTLS, as water vapor content at these altitudes depends not only on the origin of the air parcel but also on its temperature history (Fueglistaler and Haynes, 2005; Nützel et al., 2019).

CLaMS-M2 simulations (not shown) have much in common with the CLaMS-EI results with respect to the transport of monsoon tracers into the tropics. However, there are also some differences. As mentioned above, the vertical transport of the ASM
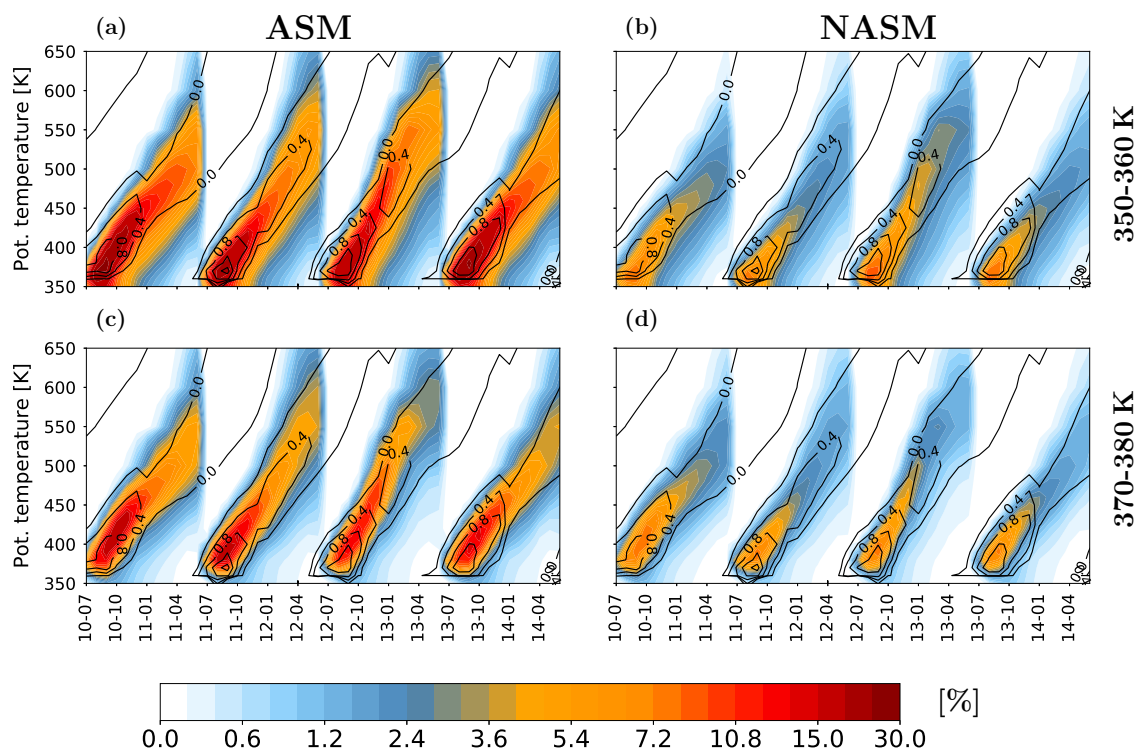
Figure 5. Potential temperature−time sections of mean monsoon air fraction (color shading) between $15°$ S and $15°$ N released in the $350−360$ K (upper; a and b) and $370−380$ K (lower; c and d) layers within the ASM (left; a and c) and NASM (right; b and d) based on CLaMS-EI simulations. Tape-recorder signals calculated from Aura MLS water vapor (in ppmv) with the annual average removed are shown as black contours for context.

210   tracers is slightly lower, with the tracers reaching slightly lower altitudes by the end of the simulation period. Perhaps linked to this slower upwelling, more monsoon air arrives in the tropics between each summer monsoon season and the following spring compared to CLaMS-EI simulations. A relatively large proportion of monsoon air is transported quasi-horizontally into the tropics before ascending to the TrP. The slower upwelling in MERRA-2 also manifests in a slight lag between the simulated monsoon tracer distribution and the MLS water vapor tape recorder signal.

215   Figure 6 shows the horizontal spread of the ASM and NASM tracers on the 400 K isentropic surface based on the CLaMS-EI simulations. Tracers initialized on both levels show broadly similar features at 400 K, although the ASM contributes much more to the lower stratosphere than does the NASM. The ASM and NASM tracers initialized at $350−360$ K are less confined in latitude, with much more transport to the SH than tracers initialized at $370−380$ K. Tracers initialized at $370−380$ K are more confined to the monsoon region and the NH. The ASM and NASM tracers coincide well with the MLS water vapor 'wet'

220   signal in the lateral tape recorder, which is again consistent with the idea that the monsoons contribute substantially to water vapor concentrations in the stratosphere. The monsoon tracer distributions based on CLaMS-M2 are more widespread than
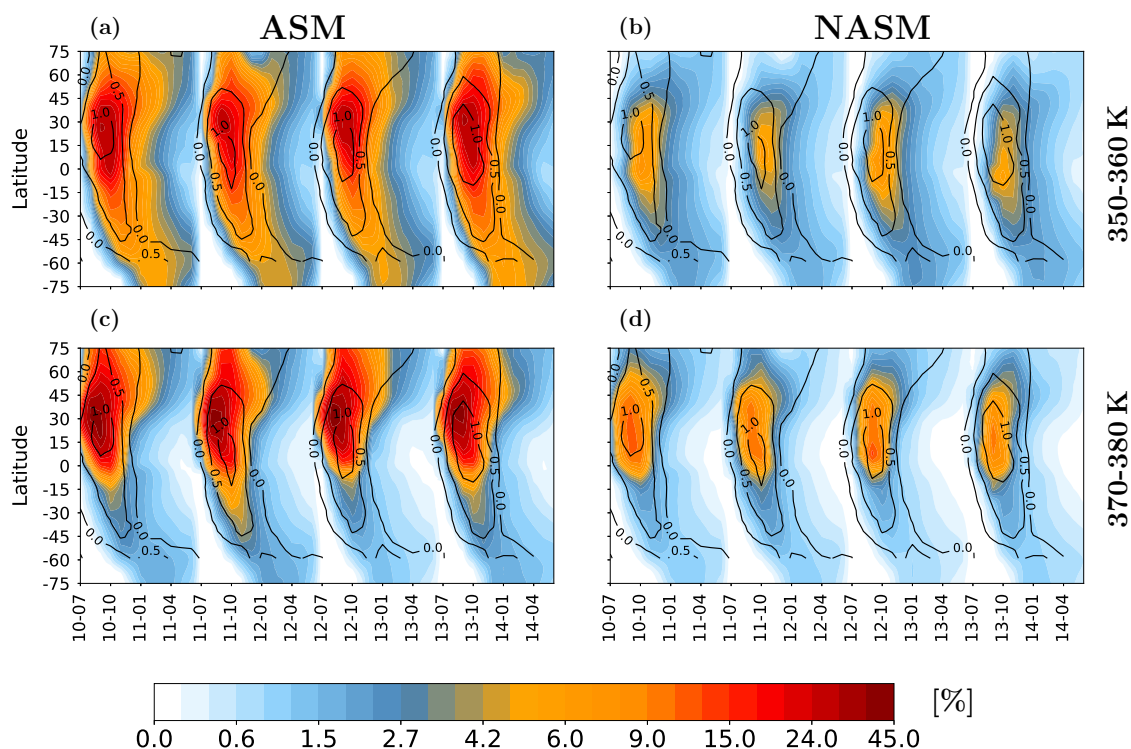
Figure 6. Zonal-mean tracer concentrations (color shading) for the ASM (left; a and c) and NASM (right; b and d) tracers initialized at $350-360$ K (upper; a and b) and $370-380$ K (lower; c and d) as functions of time and latitude on the 400 K isentropic surface based on CLaMS-EI. MLS water vapor retrievals (in ppmv) with the annual average removed are shown as black contours for context.

those based on CLaMS-EI, with a greater tendency to remain in the extratropical stratosphere regardless of the initialization level. Both sets of simulations produce close matches between the ASM and NASM tracer peaks and the 'wet' signal in MLS water vapor, indicating that horizontal transport in CLaMS-M2 is in good agreement with that in CLaMS-EI.

225   The qualitative correspondence between the monsoon tracers and the 'wet' phases of the vertical and horizontal tape recorders suggests a strong connection between stratospheric water and transport from the monsoon regions. To further investigate the extent to which the monsoon tracers can explain variability in lower stratospheric water vapor and clarify the differences between the tropical pathway and the monsoon pathway into the TrP, we correlate the monsoon tracer amounts with CLaMS-simulated concentrations of stratospheric water vapor, which have been successfully validated and used in many

230   previous studies (e.g. Rolf et al., 2018; Tao et al., 2019, and the reference therein). As shown in Fig. 7, a strong positive correlation exists between the monsoon tracers and water vapor in the tropics. Larger ASM and NASM air fractions correspond to larger water vapor mixing ratios in the tropical lower stratosphere ($420-500$ K). The distinct differences between the upper panels (tracers released in the $350-360$ K layer) and the lower panels (tracers released in the $370-380$ K layer) reflect the two transport pathways from the ASM and NASM to the tropical lower stratosphere. The right branch in Fig. 7a (Fig. 7b) mimics
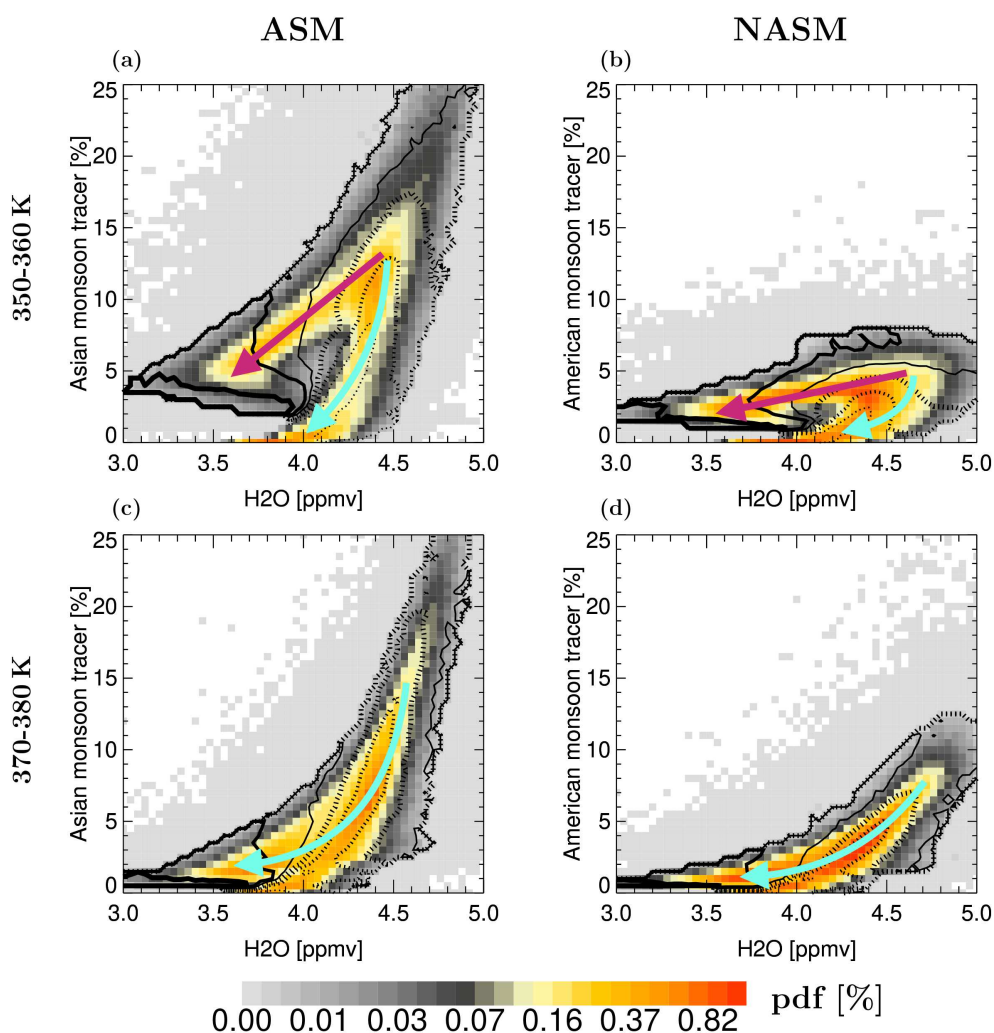
Figure 7. Correlations between CLaMS-simulated water vapor and the ASM (left; a and c) and NASM (right; b and d) tracers in the tropical stratosphere (15° S−15° N; 420−500 K) during November−May with monsoon tracers released in the 350−360 K (upper; a and b) and 370−380 K (lower; c and d) layers based on CLaMS-EI. Contours mark young air mass fractions of 24%, 33%, and 42% (from thin to thick dotted isolines) and 51%, 60%, and 69% (from thin to thick solid isolines). The cyan and magenta arrows respectively show the monsoon pathway and tropical pathway.

235 the joint distribution of ASM (NASM) tracers from 370−380 K and water vapor shown in Fig. 7c (Fig. 7d). This branch thus indicates the correlation along the monsoon transport pathway (cyan arrow), in which air ascends locally across the tropopause and then enters the tropics laterally. The left branch in Fig. 7a (Fig. 7b) is then linked to the correlation along the tropical pathway (magenta arrow), in which air from the upper troposphere above the ASM (NASM) enters the tropics quasi-horizontally before ascending via tropical upwelling. As discussed above, this tropical pathway is more common for tracers released at

240 lower altitudes (here 350−360 K). The water vapor mixing ratio along the tropical pathway is lower than that along the monsoon pathway because more dehydration is caused by the lower tropopause temperature over the tropics (figure omitted). The mass fraction of air younger than nine months is also shown in Fig. 7 (black contours) to further evaluate the vertical components of the pathways by which monsoon air reaches the tropical lower stratosphere. Young air mass fractions are considerably larger for the tropical pathway, suggesting that ascent rates over the tropics (along the tropical pathway) are much faster than

245 those over the monsoon regions (along the monsoon pathway).

4   Transport budget

In this section, we investigate the total budget and efficiencies of transport from different layers over the monsoon source regions into the global stratosphere. Three destination regions as defined in Fig. 2 are of particular interest: the tropical pipe (TrP), the extratropical lower stratosphere in the NH (LS-NH) and the extratropical lower stratosphere in the SH (LS-SH).

250 Because transport across the TTL is generally regarded as the 'main gateway into the stratosphere' (Fueglistaler et al., 2009), we compare the ASM- and NASM-related transport metrics with corresponding quantities calculated for a pure tropical source region (15° S−15° N).

4.1   Time evolution of the monsoon tracer

Figure 8a shows CLaMS-EI time series of ASM tracer in the three destination regions (TrP, LS-NH and LS-SH) defined in

255 Fig. 2. The ASM tracer initialized at 370−380 K show the largest air fraction in the LS-NH in the middle of September, with a peak value around 22%. The peak date is earlier than that shown by Ploeger et al. (2017) (peak around 15%). This is because the domain of the ASM tracer used here is larger than that based on the PV barrier definition used by Ploeger et al. (2017). Our definition of the LS-NH destination region also differs slightly from theirs. Our use of a geographical definition for the ASM as opposed to the dynamical definition used by Ploeger et al. (2017) means that some air parcels are initialized with ASM tracer

260 when they are outside of the dynamical anticyclone. These parcels reach the LS-NH much more quickly. The ASM tracers released in the 350−360 K layer show two peaks in the LS-NH. The first of these is at the beginning of September and is related to rapid isentropic poleward transport. The second occurs about one month later relative to the tracers initialized in the 370−380 K layer due to the need for additional ascent within the anticyclone. During the first three months, fewer ASM tracers released at 350−360 K are diagnosed in the LS-NH relative to ASM tracers released at 370−380 K. However, the ASM

265 tracers released at 350−360 K contribute significantly more to the composition in the LS-NH and remain in the LS-NH for longer when compared to tracers released at 370−380 K after three months. Similar transitions in the relative concentrations of
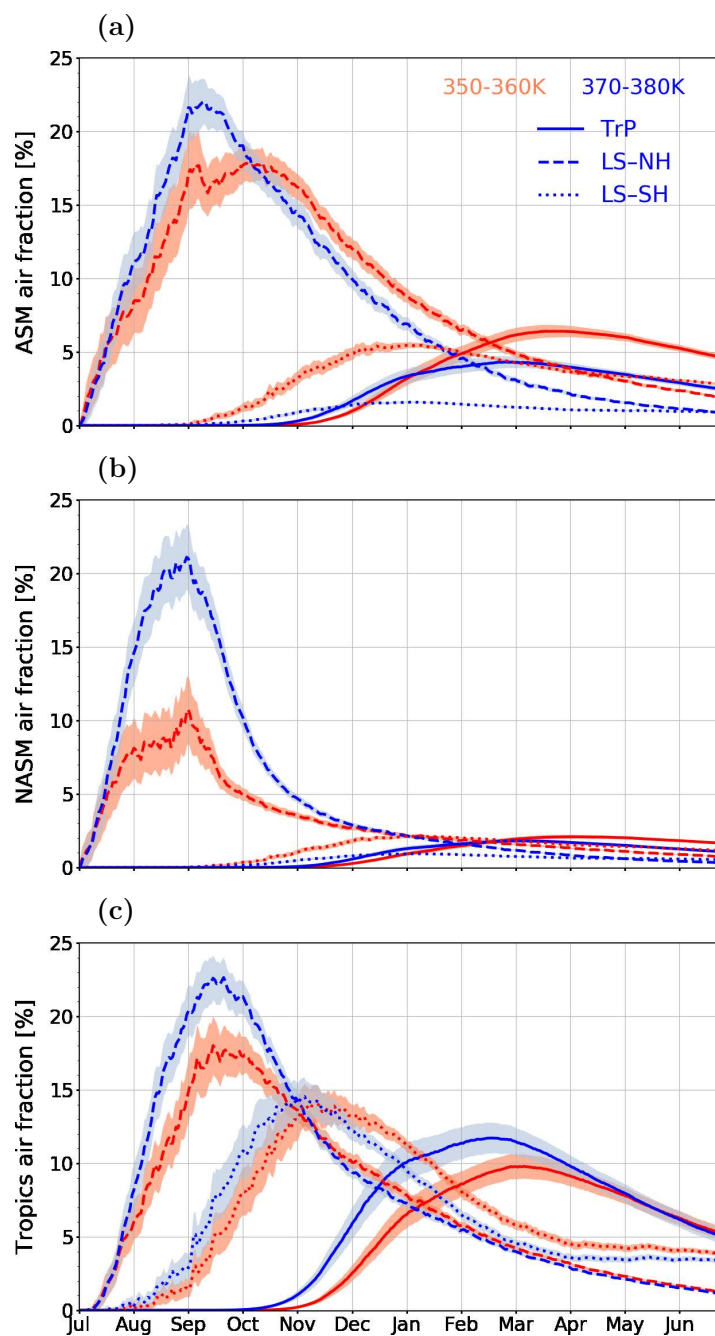
Figure 8. Climatological time series based on the CLaMS-EI simulations of three source regions: (a) ASM, (b) NASM and (c) tropics air mass fractions (in %) and diagnosed in three destination regions (see Fig. 2): tropical pipe (TrP, solid line), extratropical lower stratosphere in the NH (LS-NH, dashed line) and in the SH (LS-SH, dotted line). Shading shows the mean standard deviation in the zonal average (multiplied by 0.2 for better visibility). Red and blue lines respectively represent the tracers released in the 350−360 K and 370−380 K layer.

tracers released at $350-360\,\mathrm{K}$ and $370-380\,\mathrm{K}$ can be diagnosed in the TrP region, although the maxima are about six months later compared to that in the LS-NH. The ASM tracers start to reach the TrP region around November, peaking in the TrP around March at a value $\sim$4% for tracers released in the $370-380\,\mathrm{K}$ layer. The timing of this peak is about half a month earlier

270   than that of ASM tracers released from $350-360\,\mathrm{K}$, although the latter has a larger peak value ($\sim$7%). Tracers released at $350-360\,\mathrm{K}$ are much more abundant in the LS-SH than tracers released at $370-380\,\mathrm{K}$.

The corresponding time series of air fractions from the NASM source region to the three destination regions are illustrated in Fig. 8b. These time series show some important similarities to those based on the ASM tracers. The NASM tracers initialized in both the $350-360\,\mathrm{K}$ and $370-380\,\mathrm{K}$ layers reach their peak values in the LS-NH about two weeks earlier than the

275   corresponding ASM tracer concentrations, likely owing to the weaker dynamical confinement of NASM air in the upper troposphere. NASM tracers initialized at $370-380\,\mathrm{K}$ reach the LS-NH in much larger amounts than NASM tracers initialized at $350-360\,\mathrm{K}$, in part because the 370-380 K layer is higher than the tropopause over the NASM. However, NASM air fractions in the LS-SH and TrP are much smaller than the corresponding ASM air fractions in these regions, generally by more than a factor of 2. NASM tracers initialized at $350-360\,\mathrm{K}$ are more abundant in the three destination regions by the end relative to

280   NASM tracers initialized at $370-380\,\mathrm{K}$.

Most tropospheric air that is transported into the global stratosphere passes through the TTL via tropical upwelling. Thus, to evaluate the relative contributions of the ASM and NASM sources to the stratosphere, we use the transport of air originating in the tropics ($15° \, \mathrm{S} - 15° \, \mathrm{N}$) as a benchmark. By comparing tracers tracking air of tropical origin in the three destination regions (Fig. 8c) with those tracking air with monsoon origin in the same destination regions, we conclude that ASM tracers are as

285   abundant as tropical tracers in the LS-NH. Moreover, the abundance of the NASM tracer initialized in the $370-380\,\mathrm{K}$ layer is also comparable to the abundances of ASM or tropical tracers in the LS-NH region. Inside the TrP, the peak ASM contribution is smaller than the peak tropical contribution in early spring. However, the abundance of ASM air originating from $350-360\,\mathrm{K}$ in the TrP is comparable to that from the tropics at the end of the simulation period. Both values are about three times larger than the NASM contribution. More air in the LS-SH originates from the tropical upper troposphere than from the two monsoon

290   regions.

The time series of all source air fractions discussed above and calculated from CLaMS-M2 are very similar to those derived from CLaMS-EI (not shown). Even daily perturbations of such tracers driven by Rossby waves and diagnosed on individual isentropic surfaces show very strong similarities, as outlined later. ASM contributions based on CLaMS-M2 lag those based on CLaMS-EI by about one month, first reaching the TrP in December rather than November. This delay is related to the slower

295   tropical upwelling in MERRA-2 relative to ERA-Interim as discussed above. For the same reason, CLaMS-M2 produces larger amounts of ASM tracers in the stratosphere at the end of the simulation period. The time series of NASM tracers based on CLaMS-M2 are likewise similar to those based on CLaMS-EI, again up to and including daily variability. For the tropical source, CLaMS-M2 shows similar peak values to CLaMS-EI in the LS-SH destination region, but lower peak values in the LS-NH and TrP. However, the amount of air of tropical origin remaining in the stratosphere is larger in CLaMS-M2 than in

300   CLaMS-EI starting from the April following the July$-$August tracer release.

ERA-Interim	$340-350\,\mathrm{K}$	$350-360\,\mathrm{K}$	$360-370\,\mathrm{K}$	$370-380\,\mathrm{K}$
ASM	2.276×10^{10}	1.877×10^{10}	1.179×10^{10}	6.118×10^{9}
NASM	1.916×10^{10}	1.042×10^{10}	5.649×10^{9}	3.930×10^{9}
Tropics	8.524×10^{10}	5.484×10^{10}	3.406×10^{10}	2.207×10^{10}
MERRA-2	$340-350\,\mathrm{K}$	$350-360\,\mathrm{K}$	$360-370\,\mathrm{K}$	$370-380\,\mathrm{K}$
ASM	2.284×10^{10}	1.890×10^{10}	1.124×10^{10}	6.334×10^{9}
NASM	2.006×10^{10}	9.868×10^{9}	5.927×10^{9}	3.993×10^{9}
Tropics	8.795×10^{10}	5.420×10^{10}	3.398×10^{10}	2.254×10^{10}

Table 1. Typical masses of air contained in each box for the test experiments over the ASM, NASM and tropical source regions in CLaMS-EI (top) and CLaMS-M2 (bottom). All masses are reported in kg.

4.2 Transport efficiency

Our comparison of air fractions calculated for different transport pathways is partially hampered by the fact that the source regions have different volumes (or masses). To illustrate such differences in the domains, Table 1 shows the mass calculated for all considered source regions (ASM, NASM and tropics) based on both reanalyses. To better control for the potential influence
305 of differences in the sizes of the source domains on our quantitative estimates of transport to the stratosphere, we define the efficiency of transport (TE) using the air mass of the source domain to normalize the mass transported from each source region to the defined stratospheric destination regions. TE is defined to equal the mean source air mass fraction in the destination region times the total air mass of the destination region (e.g. TrP) divided by the air mass of the source domain (e.g. ASM).

Figure 9a compares the TE from the three source regions (ASM, NASM and Tropics) each divided into two layers ($350-360\,\mathrm{K}$
310 and $370-380\,\mathrm{K}$) to the LS-NH destination region. In contrast to the total budget, where tropical and monsoon contributions are very similar (Fig. 8), the ASM/NASM monsoons dominate the TE into the LS-NH, especially for sources in the $370-380\,\mathrm{K}$ altitude range. At the beginning, the TE is larger for the NASM than for the ASM; the larger NASM TE is in part related to the fact that the $370-380\,\mathrm{K}$ layer is above the tropopause over the NASM region and the NASM tracers are less confined. However, transport from the ASM becomes most efficient starting from October. Perhaps more surprising, the TE into the LS-SH
315 is also dominated by the ASM and NASM monsoon sources after a certain date (see Fig. 9b). For the first $4-5$ months, the TE is larger from the tropics than from the monsoon regions, especially for tracers released between $370\,\mathrm{K}$ and $380\,\mathrm{K}$. However, from January on, transport from the $350-360\,\mathrm{K}$ layers in the ASM and NASM regions reaches the LS-SH more efficiently than transport from the same layer in the tropics (with the TE slightly larger from the ASM than from the NASM). The time evolution of the source-resolved TE into the TrP is shown in Fig. 9c. Here, the highest TE values are along the pathways start-
320 ing in the ASM source region, followed by those starting in the tropical and NASM source regions. The NASM TE exceeds the
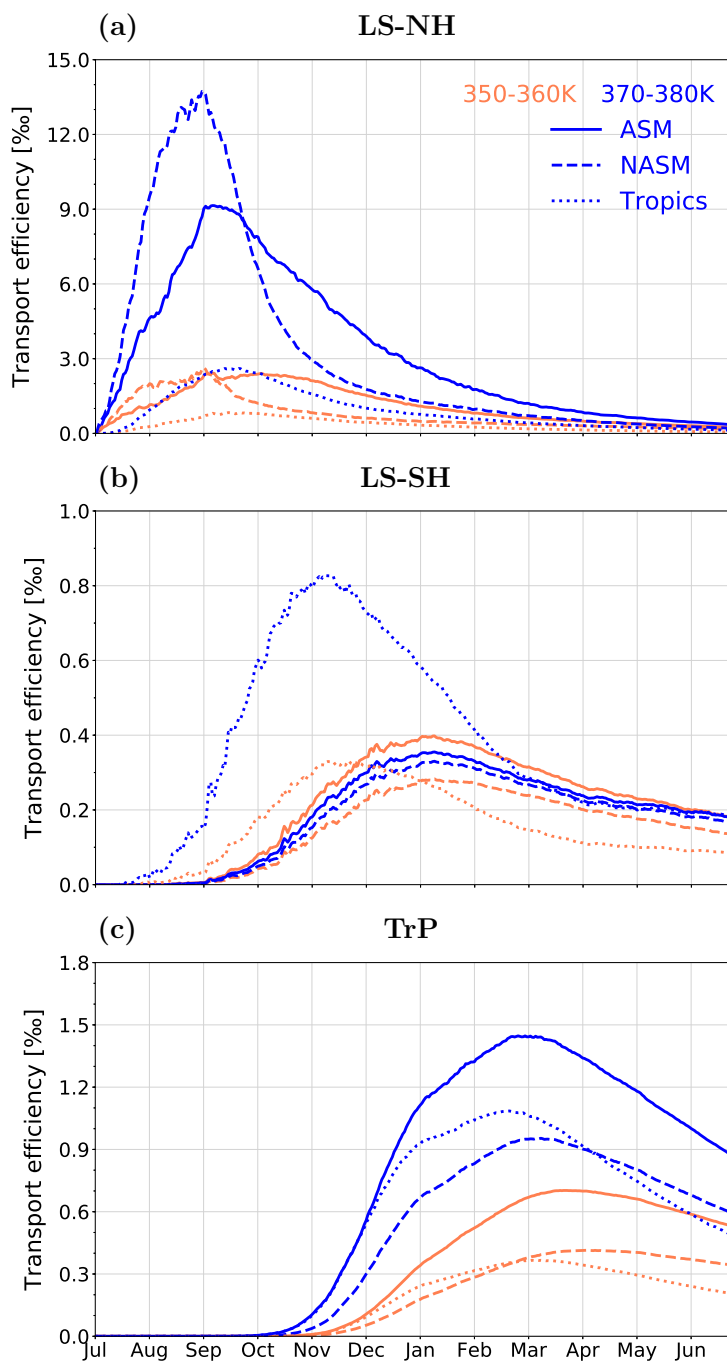
Figure 9. Climatological time series of transport efficiency (TE) as derived from the CLaMS-EI simulations and calculated for transport from the ASM (solid line), NASM (dashed line) and tropics (dotted line) source regions to the (a) LS-NH , (b) LS-SH and (c) TrP destination regions. TE (in ‰) is defined by normalizing the average monsoon or tropical air mass over the destination region by the mass of the source region. Different colors of the lines represent tracers released at different levels.
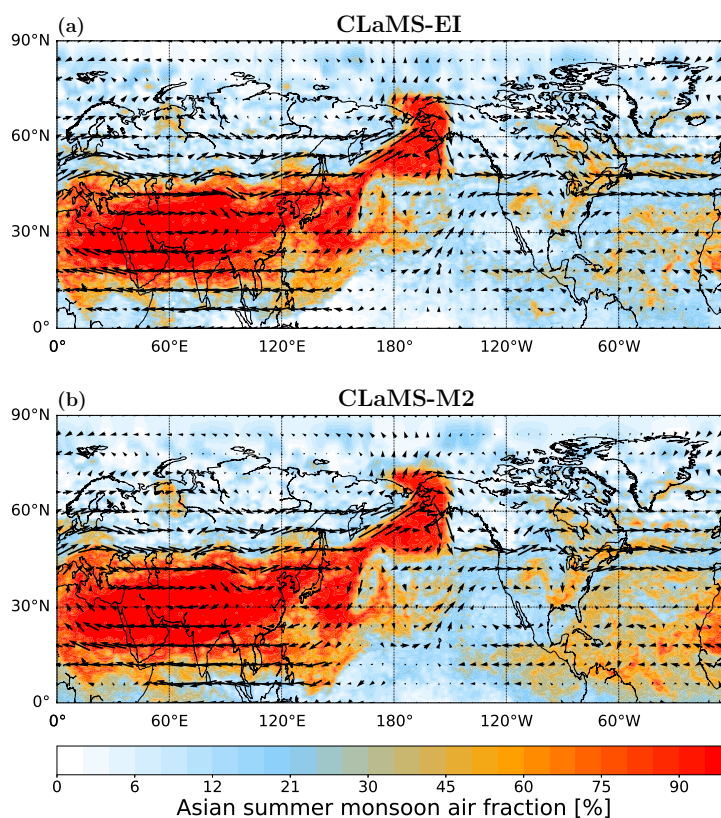
Figure 10. The distribution of (a) CLaMS-EI and (b) CLaMS-M2 tracer simulation at 380 K on 24 August 2012 initialized at 370−380 K from the ASM region. Arrows show horizontal wind. Map is created by python.

tropical TE after March for tracers from 350−360 K and after April for tracers from 370−380 K İn contrast to the total source budget (Fig. 8), transport is consistently less efficient from lower levels than from higher levels.

Patterns of TE based on CLaMS-M2 are similar to those based on CLaMS-EI (figure omitted), although there are a few important differences. First, TEs from the ASM and NASM source regions to the LS-SH destination region are much larger in CLaMS-M2 than in CLaMS-EI. Both values exceed that from the tropical source region after December (for tracers initialized at 350−360 K) or January (for tracers initialized at 370−380 K). Second, the TE to the TrP in CLaMS-M2 shows slightly higher values for both the ASM and NASM sources and lower values for tropical upwelling relative to CLaMS-EI. TE from the NASM to the TrP slightly exceeds that from the tropics to the TrP starting in March.

5 Discussion

330 We have investigated the pathways, transit times and efficiencies of transport from the ASM and NASM regions to the strato-
sphere with tracers initialized at different vertical levels using the ERA-Interim and MERRA-2 reanalyses. Both of the simula-
tions show two major pathways connecting the upper troposphere in the ASM and NASM regions to the TrP, as well as positive
correlations between monsoon air mass fractions and MLS water vapor. We have further shown that contributions from the
ASM upper troposphere ($350-360\,$K) to the TrP are comparable to those of tropical sources ten months after the release of the
335 tracers and that the most efficient transport to the TrP among the analyzed source regions is that from the ASM at $370-380\,$K.
These robust characteristics of transport in the CLaMS-EI and CLaMS-M2 simulations are based on zonal-mean metrics. To
further investigate the sensitivity of the results to the choice of reanalysis, zonally resolved results from the two sets of simu-
lations are shown in Fig. 10. Figure 10 shows distributions of ASM tracers initialized in the $370-380\,$K layer along the $380\,$K
isentropic surface on 24 August 2012. Distributions are shown for both CLaMS-EI (Fig. 10a) and CLaMS-M2 (Fig. 10b).
340 The ASM tracer is transported as far north as $75°\,$N by eddies that detach from the ASM anticyclone. This type of feature
is associated with Rossby wave breaking and can cause large fluctuations of monsoon air fraction in the LS-NH region. The
consistency between the CLaMS-EI and CLaMS-M2 results for this case again suggests good agreement between CLaMS-EI
and CLaMS-M2 with respect to horizontal transport (see also Sec. 3.2). CLaMS-EI and CLaMS-M2 also show good agreement
with respect to the horizontal distributions of monsoon tracers on other days (not shown). We select this example because it
345 represents a clear episode of Rossby wave breaking and eddy shedding.

Despite the many similarities in simulated transport from the monsoon regions to the stratosphere in CLaMS-EI and CLaMS-
M2, it has been reported elsewhere that radiative heating rates in the TTL and lower stratosphere are substantially larger
in ERA-Interim than in MERRA-2 (e.g. Ploeger et al., 2019; Tao et al., 2019). This difference directly affects the tropical
upwelling as represented in CLaMS. We have shown that the monsoon tracers reach different maximum altitudes in the TrP
350 during April$-$June in these two simulations. The stronger tropical upwelling in CLaMS-EI lifts monsoon air to higher altitudes
more quickly than the weaker tropical upwelling in CLaMS-M2. Accordingly, the transit time to a given altitude in the TrP
is slightly shorter in CLaMS-EI than in CLaMS-M2. Moreover, the smaller magnitudes of heating rates (both positive and
negative) in CLaMS-M2 tend to lead to monsoon air 'piling up' in the lowermost stratosphere and TrP. Monsoon tracers thus
retain high values in the stratosphere for longer in the CLaMS-M2 simulations. Slower cross-isentropic transport increases the
355 probability of quasi-horizontal (isentropic) transport into the tropics, where widespread upwelling helps to transport more air
upwards.

Figure 11 provides a schematic illustration of the main transport pathways from the ASM (Fig. 11a) and NASM (Fig. 11b)
source regions to the three stratospheric destination regions. The overall contributions, efficiencies and transit times along
these pathways are also listed based on the CLaMS-EI results. The greatest relative part, i.e. about 22% (18%) of the air in
360 the LS-NH consists of ASM tracers initialized at $370-380\,$K ($350-360\,$K), with an overall TE of 9‰ (2.5‰) and a transit
time of ~3 months. The contribution of the NASM tracers initialized at $370-380\,$K to the LS-NH is comparable to that of
the corresponding ASM tracers, although the contribution of the NASM tracers initialized at $350-360\,$K is much smaller than
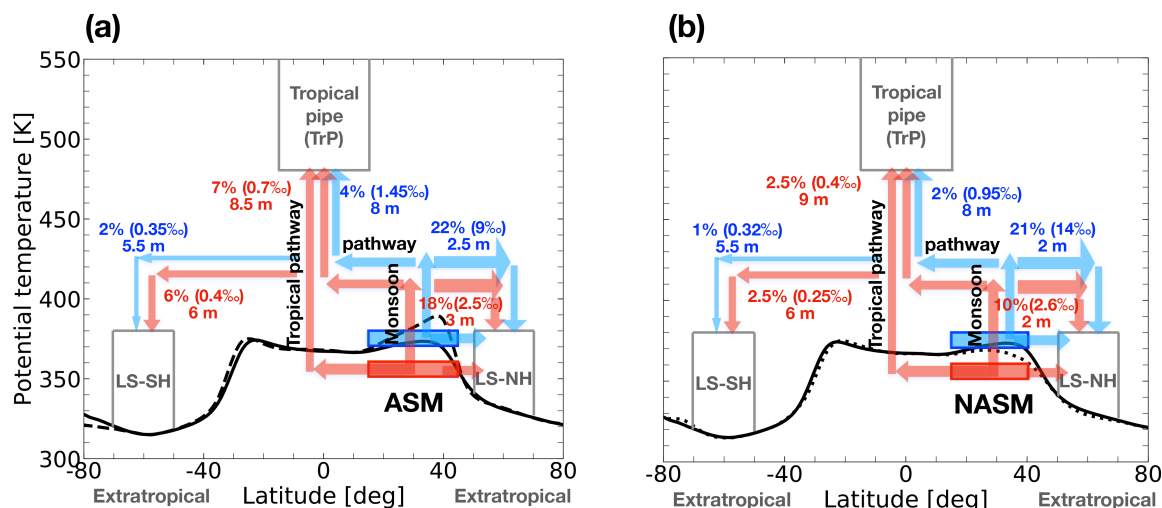
Figure 11. Schematic of tracer transport from the (a) ASM and (b) NASM region into the TrP, LS-NH and LS-SH. The red and blue boxes respectively represent the tracers initialized in the $350-360\,$K and $370-380\,$K layers. The arrows illustrate the dominant transport pathways. The numbers quantify the maximum contribution [%] (efficiency [‰]) and mean transit time [month] from the monsoon regions to the three destination regions based on the CLaMS-EI. The black solid, dashed and dotted lines respectively mark the zonal-mean, ASM and NASM tropopause (lapse rate) from ERA-Interim averaged over July−August 2010−2013.

that of the ASM tracers initialized in the same layer. Although not shown here, these three quantitative transport metrics are quite similar in CLaMS-M2 with respect to transport from the ASM and NASM regions to the LS-NH. This similarity supports

365 our contention that these two reanalyses provide very consistent representations of horizontal transport. A maximum of 7% of the air arrives in the TrP via the two main transport pathways from the $350-360\,$K layer in the ASM region. The transit time is about 8.5 months, with a peak efficiency of 0.7‰. The ASM tracers initialized at $370-380\,$K take about 8 months to arrive at the TrP. Although only about 4% of the air in the TrP comes from this source layer, the peak transport efficiency (1.45‰) is approximately twice as high as that from the $350-360\,$K layer. Transport from the source regions in the NASM

370 shows much weaker contributions to air in the TrP, along with slightly longer transit times compared to transport from the ASM. As for the NASM, the maximum contribution is larger from the $350-360\,$K layer (2.5%) but at a lower peak efficiency (0.4‰) relative to transport from the $370-380\,$K layer (2% and 0.95‰). Our results about the contributions of monsoon air to the TrP and LS-NH are respectively smaller and larger than the results from Nützel et al. (2019) because the definitions of destination regions (TrP and LS-NH) used here are quite different from theirs. Transit times from the monsoon regions to the

375 TrP are about one month longer in the CLaMS-M2 simulations than in the ClaMS-EI simulations. The overall contributions and efficiencies of transport from the ASM and NASM to the TrP are also slightly larger in CLaMS-M2 than in CLaMS-EI. The contributions from the ASM and NASM regions to the LS-SH are significantly different between tracers initialized at $350-360\,$K and tracers initialized at $370-380\,$K. In both cases, the contributions from $350-360\,$K are almost three times larger

than those from 370−380 K in CLaMS-EI. The scale of this difference is smaller in CLaMS-M2 than in CLaMS-EI. Moreover,
380   the absolute contributions based on CLaMS-M2 are much larger, with higher transport efficiencies and slightly longer transit
times relative to CLaMS-EI. Since the tracers in the simulations are reset every July, we cannot infer how differences between
CLaMS-EI and CLaMS-M2 evolve after June. However, based on the tendencies toward the end of the simulation period,
the concentrations of monsoon tracers in the stratosphere in CLaMS-M2 may decrease further in time, coming into better
agreement with CLaMS-EI, until the point when the signature of the new monsoon season arrives.

6   Conclusions

Both the CLaMS-EI and CLaMS-M2 simulations show that transport from the upper troposphere (350−360 K) over ASM
and NASM regions makes a larger contribution to the TrP relative to transport from just below the tropopause (370−380 K).
This difference is related to the mass of air within each layer, which is larger for 350−360 K layer than for the 370−380 K
layer above the monsoon regions. Differences in the contributions of the two layers also arise due to vertical differences in the
390   dynamical situation. Monsoon air mass fractions in the LS-SH during the following April−June are larger for tracers released
at lower levels, reflecting weaker confinement by the anticyclone in the upper troposphere. By contrast, monsoon air fractions
in the LS-NH region during the following April−June are larger for tracers released at higher levels, reflecting the importance
of wave-driven transport of tracers that reach the extratropical lower stratosphere quasi-isentropically at higher levels.

Peak values of monsoon tracers in the tropical stratosphere are in good agreement with the 'wet' phase of the water vapor
395   tape recorder based on Aura MLS, which is consistent with the monsoon regions playing an influential role in the seasonal
cycle of water vapor in the tropical lower stratosphere. Differences between simulations with tracers initialized at 350−360 K
and simulations with tracers initialized at 370−380 K suggest the existence of two main transport pathways between the
monsoon regions and the TrP. The first pathway (tropical pathway) involves the quasi-horizontal transport of monsoon air into
the tropics, where that air then ascends into the stratosphere via tropical upwelling. The second pathway (monsoon pathway)
400   involves the ascent of monsoon air within the monsoon anticyclone into the lower stratosphere, where it is then transported
quasi-horizontally to the tropical lower stratosphere. Both pathways ultimately reach the TrP. However, the greater abundance
of relatively young air along the tropical (first) pathway suggests that vertical transport is faster along this route than along the
monsoon (second) pathway.

CLaMS-EI and CLaMS-M2 consistently indicate that the ultimate contribution of air mass transport from the ASM upper
405   troposphere (350−360 K) to the TrP (∼5%) is comparable to that of direct ascent from the inner tropics (15° S−15° N) ten
months after the release of the source tracers. These two contributions are approximately three times larger than the air mass
contribution from the NASM (∼1.5%) to the TrP at the end of the simulation period. To help eliminate the influence of the
origin region size on our quantitative transport estimates, we calculate normalized transport efficiencies by dividing the total
air mass transport by the average mass of air within the source domain. The ASM region at 370−380 K shows the highest TE
410   to the TrP (0.9‰). Meanwhile, the TE from the NASM to the TrP is similar to the TE from the tropics to the TrP (0.3−0.6‰).
These values are approximately half that of the TE from the ASM to the TrP.

Our results further confirm the important role of the ASM anticyclone in troposphere-to-stratosphere transport. Although the contribution from the NASM region to the TrP is less than the contributions from the ASM or from the tropics, it is still influential at about one third of the contribution from ASM. Moreover, the TE from the NASM to the TrP is as high as that of direct upwelling within the tropics during the boreal summer season.

Author contributions. XY carried out the ERA-Interim and MERRA-2 driven model simulations and the data analysis. PK, FP and AP contributed codes for the analysis. JW contributed codes to prepare the MERRA-2 reanalysis data. PK, FP and AP contributed to the design of the analysis. PK, FP, AP, JW, RM, MR provided helpful discussions and comments. XY wrote the paper with contributions from all co-authors.

Competing interests. TEXT

Acknowledgements. This research was partially supported by the National Key Research and development program of China (2018YFC1505703), the National Science Foundation of China (91837311), and a joint DFG-NSFC research project with DFG project number 392169209 and NSFC project number 20171352419. We thank the European Centre for Medium-Range Weather Forecasts (ECMWF) and National Aeronautics and Space Admistration (NASA) for providing ERA-Interim and MERRA-2 meteorological reanalysis data for this study. We thank MLS for providing CO and H_2O data, and ACE-FTS team for providing HCN data. The MLS and ACE-FTS data are available at http://mirador.gsfc.nasa.gov and http://www.ace.uwaterloo.ca/data.php, respectively.

References

Abalos, M., Legras, B., Ploeger, F., and Randel, W. J.: Evaluating the advective Brewer-Dobson circulation in three reanalyses for the period 1979-2012, J. Geophys. Res., 120, doi:10.1002/2015JD023 182, 2015.

430 Bergman, J. W., Jensen, E. J., Pfister, L., and Yang, Q.: Seasonal differences of vertical-transport efficiency in the tropical tropopause layer: On the interplay between tropical deep convection, large-scale vertical ascent, and horizontal circulations, J. Geophys. Res., 117, https://doi.org/10.1029/2011JD016992, 2012.

Bergman, J. W., Fierli, F., Jensen, E. J., Honomichl, S., and Pan, L. L.: Boundary layer sources for the Asian anticyclone: Regional contributions to a vertical conduit, J. Geophys. Res., 118, 2560–2575, https://doi.org/10.1002/jgrd.50142, 2013.

435 Bernath, P. F., McElroy, C. T., Abrams, M. C., Boone, C. D., Butler, M., Camy-Peyret, C., Carleer, M., Clerbaux, C., Coheur, P.-F., Colin, R., DeCola, P., DeMazière, M., Drummond, J. R., Dufour, D., Evans, W. F. J., Fast, H., Fussen, D., Gilbert, K., Jennings, D. E., Llewellyn, E. J., Lowe, R. P., Mahieu, E., McConnell, J. C., McHugh, M., McLeod, S. D., Michaud, R., Midwinter, C., Nassar, R., Nichitiu, F., Nowlan, C., Rinsland, C. P., Rochon, Y. J., Rowlands, N., Semeniuk, K., Simon, P., Skelton, R., Sloan, J. J., Soucy, M.-A., Strong, K., Tremblay, P., Turnbull, D., Walker, K. A., Walkty, I., Wardle, D. A., Wehrle, V., Zander, R., and Zou, J.: Atmospheric Chemistry

440 Experiment (ACE) Mission overview, Geophys. Res. Lett., 32, L15S01, https://doi.org/10.1029/2005GL022386, 2005.

Boone, C. D., Nassar, R., Walker, K. A., Rochon, Y., McLeod, S. D., Rinsland, C. P., and Bernath, P. F.: Retrievals for the atmospheric chemistry experiment Fourier-transform spectrometer, Applied optics, 44, 7218–7231, 2005.

Boone, C. D., Walker, K. A., and Bernath, P. F.: Version 3 Retrievals for the Atmospheric Chemistry Experiment Fourier Transform Spectrometer (ACE-FTS), (Peter F. Bernath, editor, A. Deepak Publishing, Hampton, Virginia, U.S.A., 2013), 2013.

445 Brunamonti, S., Jorge, T., Oelsner, P., Hanumanthu, S., Singh, B. B., Kumar, K. R., Sonbawne, S., Meier, S., Singh, D., Wienhold, F. G., Luo, B. P., Boettcher, M., Poltera, Y., Jauhiainen, H., Kayastha, R., Karmacharya, J., Dirksen, R., Naja, M., Rex, M., Fadnavis, S., and Peter, T.: Balloon-borne measurements of temperature, water vapor, ozone and aerosol backscatter on the southern slopes of the Himalayas during StratoClim 2016–2017, Atmospheric Chemistry and Physics, 18, 15 937–15 957, https://doi.org/10.5194/acp-18-15937-2018, https://www.atmos-chem-phys.net/18/15937/2018/, 2018.

450 Chen, P.: Isentropic cross-tropopause mass exchange in the extratropics, Journal of Geophysical Research: Atmospheres, 100, 16 661–16 673, https://doi.org/10.1029/95JD01264, https://agupubs.onlinelibrary.wiley.com/doi/abs/10.1029/95JD01264, 1995.

Dee, D. P., Uppala, S. M., Simmons, A. J., Berrisford, P., Poli, P., Kobayashi, S., Andrae, U., Balmaseda, M. A., Balsamo, G., Bauer, P., Bechtold, P., Beljaars, A. C. M., van de Berg, L., Bidlot, J., Bormann, N., Delsol, C., Dragani, R., Fuentes, M., Geer, A. J., Haimberger, L., Healy, S. B., Hersbach, H., Holm, E. V., Isaksen, L., Kallberg, P., Koehler, M., Matricardi, M., McNally, A. P., Monge-Sanz, B. M., Mor-

455 crette, J.-J., Park, B.-K., Peubey, C., de Rosnay, P., Tavolato, C., Thepaut, J.-N., and Vitart, F.: The ERA-Interim reanalysis: configuration and performance of the data assimilation system, Q. J. R. Meteorol. Soc., 137, 553–597, https://doi.org/10.1002/qj.828, 2011.

Dessler, A. E. and Sherwood, S. C.: Effect of convection on the summertime extratropical lower stratosphere, J. Geophys. Res., 109, D23301, 2004.

Dethof, A., O'Neill, A., Slingo, J. M., and Smit, H. G. J.: A mechanism for moistening the lower stratosphere involving the Asian summer

460 monsoon, Q. J. R. Meteorol. Soc., 556, 1079–1106, 1999.

Dunkerton, T. J.: Evidence of meridional motion in the summer lower stratosphere adjacent to monsoon regions, J. Geophys. Res., 100, 16,675–16,688, 1995.

Eluszkiewicz, J., Hemler, R., Mahlman, J., Bruhwiler, L., and Takacs, L.: Sensitivity of age-of-air calculations to the choice of advection scheme, J. Atmos. Sci., 57, 3185–3201, 2000.

465   Fadnavis, S., Semeniuk, K., Schultz, M. G., Kiefer, M., Mahajan, A., Pozzoli, L., and Sonbawane, S.: Transport pathways of peroxyacetyl nitrate in the upper troposphere and lower stratosphere from different monsoon systems during the summer monsoon season, Atmospheric Chemistry and Physics, 15, 11 477–11 499, https://doi.org/10.5194/acp-15-11477-2015, https://www.atmos-chem-phys.net/15/11477/2015/, 2015.

Fu, R., Hu, Y., Wright, J. S., Jiang, J. H., Dickinson, R. E., Chen, M., Filipiak, M., Read, W. G., Waters, J. W., and Wu, D. L.: Short circuit
470   of water vapor and polluted air to the global stratosphere by convective transport over the Tibetan Plateau, Proceedings of the National Academy of Sciences, 103, 5664–5669, https://doi.org/10.1073/pnas.0601584103, http://www.pnas.org/content/103/15/5664, 2006.

Fueglistaler, S. and Haynes, P. H.: Control of interannual and longer-term variability of stratospheric water vapor, J. Geophys. Res., 110, D24108, https://doi.org/10.1029/2005JD006019, 2005.

Fueglistaler, S., Dessler, A. E., Dunkerton, T. J., Folkins, I., Fu, Q., and Mote, P. W.: Tropical tropopause layer, Rev. Geophys., 47, RG1004,
475   https://doi.org/10.1029/2008RG000267, 2009.

Garny, H. and Randel, W. J.: Transport pathways from the Asian monsoon anticyclone to the stratosphere, Atmospheric Chemistry and Physics, 16, 2703–2718, https://doi.org/10.5194/acp-16-2703-2016, https://www.atmos-chem-phys.net/16/2703/2016/, 2016.

Gettelman, A., Fujiwara, P. M. d. F., Fu, Q., Vömel, H., Gohar, L. K., Johanson, C., and Aaammerman, M.: Radiation balance of the tropical
480   tropopause layer, J. Geophys. Res., 109, https://doi.org/10.1029/2003JD004190, 2004a.

Gettelman, A., Kinnison, D., Dunkerton, T. J., and Brasseur, G. P.: Impact of monsoon circulations on the upper troposphere and lower stratosphere, J. Geophys. Res., 109, D22101, https://doi.org/10.1029/2004JD004878, warning: BibtexKey has changed!!, 2004b.

Haynes, P. and Shuckburgh, E.: Effective diffusivity as a diagnostic of atmospheric transport, 2, Troposphere and lower stratosphere, J. Geophys. Res., 105, 22 795–22 810, 2000.

485   Konopka, P., Steinhorst, H.-M., Grooß, J.-U., Günther, G., Müller, R., Elkins, J. W., Jost, H.-J., Richard, E., Schmidt, U., Toon, G., and McKenna, D. S.: Mixing and Ozone Loss in the 1999-2000 Arctic Vortex: Simulations with the 3-dimensional Chemical Lagrangian Model of the Stratosphere (CLaMS), J. Geophys. Res., 109, D02315, https://doi.org/10.1029/2003JD003792, 2004.

Konopka, P., Ploeger, F., Tao, M., Birner, T., and Riese, M.: Hemispheric asymmetries and seasonality of mean age of air in the lower stratosphere: Deep versus shallow branch of the Brewer-Dobson circulation, J. Geophys. Res., 120, 2053–2066,
490   https://doi.org/10.1002/2014JD022429, 2015.

Li, D., Vogel, B., Müller, R., Bian, J., Günther, G., Li, Q., Zhang, J., Bai, Z., Vömel, H., and Riese, M.: High tropospheric ozone in Lhasa within the Asian summer monsoon anticyclone in 2013: influence of convective transport and stratospheric intrusions, Atmospheric Chemistry and Physics, 18, 17 979–17 994, https://doi.org/10.5194/acp-18-17979-2018, https://www.atmos-chem-phys.net/18/17979/2018/, 2018.

495   Liang, Q., Jaeglé, L., Jaffe, D. A., Weiss-Penzias, P., Heckman, A., and Snow, J. A.: Long-range transport of Asian pollution to the northeast Pacific: Seasonal variations and transport pathways of carbon monoxide, Journal of Geophysical Research: Atmospheres, 109, https://doi.org/10.1029/2003JD004402, https://agupubs.onlinelibrary.wiley.com/doi/abs/10.1029/2003JD004402, 2004.

Livesey, N. J., Read, W. G., Wagner, P. A., Froidevaux, L., Lambert, A., Manney, G. L., Valle, L. F. M., Pumphrey, H. C., Santee, M. L., Schwartz, M. J., Wang, S., Fuller, R. A., Jarnot, R. F., Knosp, B. W., and Martinez, E.: Version 4.2x Level 2 data quality and description
500   document, https://mls.jpl.nasa.gov/data/v4-2_data_quality_document.pdf, 2018.

McKenna, D. S., Konopka, P., Grooß, J.-U., Günther, G., Müller, R., Spang, R., Offermann, D., and Orsolini, Y.: A new Chemical Lagrangian Model of the Stratosphere (CLaMS): 1. Formulation of advection and mixing, J. Geophys. Res., 107, 4309, https://doi.org/10.1029/2000JD000114, 2002.

Mote, P. W., Rosenlof, K. H., McIntyre, M. E., Carr, E. S., Gille, J. G., Holton, J. R., Kinnersley, J. S., Pumphrey, H. C., Russell III, J. M., and Waters, J. W.: An atmospheric tape recorder: The imprint of tropical tropopause temperatures on stratospheric water vapor, J. Geophys. Res., 101, 3989 – 4006, 1996.

Nützel, M., Podglajen, A., Garny, H., and Ploeger, F.: Quantification of water vapour transport from the Asian monsoon to the stratosphere, Atmospheric Chemistry and Physics, 19, 8947–8966, https://doi.org/10.5194/acp-19-8947-2019, https://www.atmos-chem-phys.net/19/8947/2019/, 2019.

Orbe, C., Holzer, M., Polvani, L. M., and Waugh, D.: Air-mass origin as a diagnostic of tropospheric transport, J. Geophys. Res., 118, 1459–1470, https://doi.org/10.1002/jgrd.50133, 2013.

Pan, L. L., Honomichl, S. B., Kinnison, D. E., Abalos, M., Randel, W. J., Bergman, J. W., and Bian, J.: Transport of chemical tracers from the boundary layer to stratosphere associated with the dynamics of the Asian summer monsoon, Journal of Geophysical Research: Atmospheres, 121, 14,159–14,174, https://doi.org/10.1002/2016JD025616, https://agupubs.onlinelibrary.wiley.com/doi/abs/10.1002/2016JD025616, 2016.

Park, M., Randel, W. J., Emmons, L. K., Bernath, P. F., Walker, K. A., and Boone, C. D.: Chemical isolation in the Asian monsoon anticyclone observed in Atmospheric Chemistry Experiment (ACE-FTS) data, Atmos. Chem. Phys., 8, 757–764, 2008.

Park, M., Randel, W. J., Emmons, L. K., and Livesey, N. J.: Transport pathways of carbon monoxide in the Asian summer monsoon diagnosed from Model of Ozone and Related Tracers (MOZART), J. Geophys. Res., 114, D08303, https://doi.org/10.1029/2008JD010621, 2009.

Ploeger, F., Günther, G., Konopka, P., Fueglistaler, S., Müller, R., Hoppe, C., Kunz, A., Spang, R., Grooß, J.-U., and Riese, M.: Horizontal water vapor transport in the lower stratosphere from subtropics to high latitudes during boreal summer, J. Geophys. Res., 118, 8111–8127, https://doi.org/10.1002/jgrd.50636, 2013.

Ploeger, F., Riese, M., Haenel, F., P.Konopka, Müller, R., and Stiller, G.: Variability of stratospheric mean age of air and of the local effects of residual circulation and eddy mixing, J. Geophys. Res., 120, 716–733, https://doi.org/10.1002/2014JD022468, 2015.

Ploeger, F., Konopka, P., Walker, K., and Riese, M.: Quantifying pollution transport from the Asian monsoon anticyclone into the lower stratosphere, Atmos. Chem. Phys., 16, 7055–7066, https://doi.org/10.5194/acp-17-7055-2017, 2017.

Ploeger, F., Legras, B., Charlesworth, E., Yan, X., Diallo, M., Konopka, P., Birner, T., Tao, M., Engel, A., and Riese, M.: How robust are stratospheric age of air trends from different reanalyses?, Atmospheric Chemistry and Physics, 19, 6085–6105, https://doi.org/10.5194/acp-19-6085-2019, https://www.atmos-chem-phys.net/19/6085/2019/, 2019.

Pommrich, R., Müller, R., Grooß, J.-U., Konopka, P., Ploeger, F., Vogel, B., Tao, M., Hoppe, C. M., Günther, G., Spelten, N., Hoffmann, L., Pumphrey, H.-C., Viciani, S., D'Amato, F., Volk, C. M., Hoor, P., Schlager, H., and Riese, M.: Tropical troposphere to stratosphere transport of carbon monoxide and long-lived trace species in the Chemical Lagrangian Model of the Stratosphere (CLaMS), Geoscientific Model Development, 7, 2895–2916, https://doi.org/10.5194/gmd-7-2895-2014, http://www.geosci-model-dev.net/7/2895/2014/, 2014.

Poshyvailo, L., Müller, R., Konopka, P., Günther, G., Riese, M., Podglajen, A., and Ploeger, F.: Sensitivities of modelled water vapour in the lower stratosphere: temperature uncertainty, effects of horizontal transport and small-scale mixing, Atmospheric Chemistry and Physics, 18, 8505–8527, 2018.

Randel, W. and Jensen, E.: Physical processes in the tropical tropopause layer and their role in a changing climate, Nature Geoscience, 6, 169–176, https://doi.org/10.1038/ngeo1733, 2013.

Randel, W. J. and Park, M.: Deep convective influence on the Asian summer monsoon anticyclone and associated tracer variability observed
540   with Atmospheric Infrared Sounder (AIRS), J. Geophys. Res., 111, D12314, https://doi.org/10.1029/2005JD006490, 2006.

Randel, W. J., Wu, F., Gettelman, A., Russell, J., Zawodny, J., and Oltmans, S.: Seasonal variation of water vapor in the lower stratosphere
    observed in Halogen Occultation Experiment data, J. Geophys. Res., 106, D13, https://doi.org/10.1029/2001JD900048, 2001.

Randel, W. J., Park, M., Emmons, L., Kinnison, D., Bernath, P., Walker, K. A., Boone, C., and Pumphrey, H.: Asian Monsoon Transport of
    Pollution to the Stratosphere, Science, 328, 611–613, https://doi.org/10.1126/science.1182274, 2010.

545 Randel, W. J., Moyer, E., Park, M., Jensen, E., Bernath, P., Walker, K., and Boone, C.: Global variations of HDO and HDO/H_2O ra-
    tios in the upper troposphere and lower stratosphere derived from ACE–FTS satellite measurements, J. Geophys. Res., 117, D06303,
    https://doi.org/10.1029/2011JD016632, 2012.

Rolf, C., Vogel, B., Hoor, P., Afchine, A., Günther, G., Krämer, M., Müller, R., Müller, S., Spelten, N., and Riese, M.: Water vapor increase in
    the lower stratosphere of the Northern Hemisphere due to the Asian monsoon anticyclone observed during the TACTS/ESMVal campaigns,
550   Atmospheric Chemistry and Physics, 18, 2973–2983, 2018.

Rosenlof, K. H.: Seasonal cycle of the residual mean meridional circulation in the stratosphere, J. Geophys. Res., 100, 5173 – 5191, 1995.

Santee, M. L., Manney, G. L., Livesey, N. J., Schwartz, M. J., Neu, J. L., and Read, W. G.: A comprehensive overview
    of the climatological composition of the Asian summer monsoon anticyclone based on 10 years of Aura Microwave Limb
    Sounder measurements, Journal of Geophysical Research: Atmospheres, 122, 5491–5514, https://doi.org/10.1002/2016JD026408,
555   https://agupubs.onlinelibrary.wiley.com/doi/abs/10.1002/2016JD026408, 2017.

Schoeberl, M. R., Douglass, A. R., Zhu, Z. X., and Pawson, S.: A comparison of the lower stratospheric age spectra derived from a general
    circulation model and two data assimilation systems, J. Geophys. Res., 108, 4113, https://doi.org/10.1029/2002JD002652, 2003.

Schoeberl, M. R., Dessler, A. E., and Wang, T.: Simulation of stratospheric water vapor and trends using three reanalyses, Atmos. Chem.
    Phys., 12, 6475–6487, https://doi.org/10.5194/acp-12-6475-2012, 2012.

560 Tao, M., Konopka, P., Ploeger, F., Yan, X., Wright, J. S., Diallo, M., Fueglistaler, S., and Riese, M.: Multitimescale variations in mod-
    eled stratospheric water vapor derived from three modern reanalysis products, Atmospheric Chemistry and Physics, 19, 6509–6534,
    https://doi.org/10.5194/acp-19-6509-2019, https://www.atmos-chem-phys.net/19/6509/2019/, 2019.

Tweedy, O. V., Waugh, D. W., Randel, W. J., Abalos, M., Oman, L. D., and Kinnison, D. E.: The Impact of Boreal Sum-
    mer ENSO Events on Tropical Lower Stratospheric Ozone, Journal of Geophysical Research: Atmospheres, 123, 9843–9857,
565   https://doi.org/10.1029/2018JD029020, https://agupubs.onlinelibrary.wiley.com/doi/abs/10.1029/2018JD029020, 2018.

Ungermann, J., Ern, M., Kaufmann, M., Müller, R., Spang, R., Ploeger, F., Vogel, B., and Riese, M.: Observations of PAN and its con-
    finement in the Asian summer monsoon anticyclone in high spatial resolution, Atmospheric Chemistry and Physics, 16, 8389–8403,
    https://doi.org/10.5194/acp-16-8389-2016, https://www.atmos-chem-phys.net/16/8389/2016/, 2016.

Vernier, J.-P., Thomason, L. W., and Kar, J.: CALIPSO detection of an Asian tropopause aerosol layer, Geophys. Res. Lett., 38, L07804,
570   https://doi.org/10.1029/2010GL046614, 2011.

Vernier, J. P., Fairlie, T. D., Natarajan, M., Wienhold, F. G., Bian, J., Martinsson, B. G., Crumeyrolle, S., Thomason, L. W., and Bedka, K. M.:
    Increase in upper tropospheric and lower stratospheric aerosol levels and its potential connection with Asian pollution, J. Geophys. Res.,
    https://doi.org/10.1002/2014JD022372, 2015.

Vernier, J.-P., Fairlie, T. D., Deshler, T., Venkat Ratnam, M., Gadhavi, H., Kumar, B. S., Natarajan, M., Pandit, A. K., Akhil Raj, S. T.,
575   Hemanth Kumar, A., Jayaraman, A., Singh, A. K., Rastogi, N., Sinha, P. R., Kumar, S., Tiwari, S., Wegner, T., Baker, N., Vignelles, D.,
    Stenchikov, G., Shevchenko, I., Smith, J., Bedka, K., Kesarkar, A., Singh, V., Bhate, J., Ravikiran, V., Durga Rao, M., Ravindrababu,

S., Patel, A., Vernier, H., Wienhold, F. G., Liu, H., Knepp, T. N., Thomason, L., Crawford, J., Ziemba, L., Moore, J., Crumeyrolle, S., Williamson, M., Berthet, G., Jégou, F., and Renard, J.-B.: BATAL: The Balloon Measurement Campaigns of the Asian Tropopause Aerosol Layer, Bulletin of the American Meteorological Society, 99, 955–973, 2018.

580 Vogel, B., Günther, G., Müller, R., Grooß, J.-U., Hoor, P., Krämer, M., Müller, S., Zahn, A., and Riese, M.: Fast transport from Southeast Asia boundary layer sources to northern Europe: rapid uplift in typhoons and eastward eddy shedding of the Asian monsoon anticyclone, Atmos. Chem. Phys., 14, 12 745–12 762, https://doi.org/10.5194/acp-14-12745-2014, http://www.atmos-chem-phys.net/14/12745/2014/, 2014.

Vogel, B., Günther, G., Müller, R., Grooß, J.-U., Afchine, A., Bozem, H., Hoor, P., Krämer, M., Müller, S., Riese, M., Rolf, C., Spelten,
585 N., Stiller, G. P., Ungermann, J., and Zahn, A.: Long-range transport pathways of tropospheric source gases originating in Asia into the northern lower stratosphere during the Asian monsoon season 2012, Atmospheric Chemistry and Physics, 16, 15 301–15 325, 2016.

Vogel, B., Müller, R., Günther, G., Spang, R., Hanumanthu, S., Li, D., Riese, M., and Stiller, G. P.: Lagrangian simulations of the transport of young air masses to the top of the Asian monsoon anticyclone and into the tropical pipe, Atmospheric Chemistry and Physics, 19, 6007–6034, https://doi.org/10.5194/acp-19-6007-2019, https://www.atmos-chem-phys.net/19/6007/2019/, 2019.

590 Wang, T., Randel, W. J., Dessler, A. E., Schoeberl, M. R., and Kinnison, D. E.: Trajectory model simulations of ozone (O_3) and carbon monoxide (CO) in the lower stratosphere, Atmospheric Chemistry and Physics, pp. 7135–7147, https://doi.org/10.5194/acp-14-7135-2014, 2014.

Wright, J. S. and Fueglistaler, S.: Large differences in reanalyses of diabatic heating in the tropical upper troposphere and lower stratosphere, Atmos. Chem. Phys., 13, 9565–9576, https://doi.org/10.5194/acp-13-9565-2013, 2013.

595 Wright, J. S., Fu, R., Fueglistaler, S., Liu, Y. S., and Zhang, Y.: The influence of summertime convection over Southeast Asia on water vapor in the tropical stratosphere, J. Geophys. Res., 116, D12302, https://doi.org/10.1029/2010JD015416, 2011.

Yan, X., Konopka, P., Ploeger, F., Tao, M., Müller, R., Santee, M. L., Bian, J., and Riese, M.: El Niño Southern Oscillation influence on the Asian summer monsoon anticyclone, Atmospheric Chemistry and Physics, pp. 8079–8096, https://doi.org/10.5194/acp-18-8079-2018, 2018.

600 Yu, P., Rosenlof, K. H., Liu, S., Telg, H., Thornberry, T. D., Rollins, A. W., Portmann, R. W., Bai, Z., Ray, E. A., Duan, Y., Pan, L. L., Toon, O. B., Bian, J., and Gao, R.-S.: Efficient transport of tropospheric aerosol into the stratosphere via the Asian summer monsoon anticyclone, Proceedings of the National Academy of Sciences, pp. 6972–6977, https://doi.org/10.1073/pnas.1701170114, 2017.